Received: 7 December 2022 | Revised: 23 March 2023 | Accepted: 27 March 2023

DOI: 10.1002/apj.2910

RESEARCH ARTICLE

Asia-Pacific Journal of Chemical Engineering | Curtin University | WILEY

Suspension of a single sphere in a stirred tank with transitional flow

Jianghao Wang[1,2] | Fenglei Huang[3] | Kun Zhang[1,2] | Chao Wang[1,2] | Zhipeng Li[1,2] | Zhengming Gao[1,2] | Jos Derksen[4]

[1]Beijing Advanced Innovation Center for Soft Matter Science and Engineering, Beijing University of Chemical Technology, Beijing 100029, China

[2]State Key Laboratory of Chemical Resource Engineering, School of Chemical Engineering, Beijing University of Chemical Technology, Beijing 100029, China

[3]China National Bluestar (Group) Co, Ltd, Beijing 100029, China

[4]School of Engineering, University of Aberdeen, Aberdeen AB24 3UE, UK

Correspondence
Zhipeng Li and Zhengming Gao, Beijing Advanced Innovation Center for Soft Matter Science and Engineering, Beijing University of Chemical Technology, Beijing 100029, China.
Email: lizp@buct.edu.cn and gaozm@buct.edu.cn

Abstract

The lift-off characteristics of a single spherical particle in a stirred tank with transitional flow generated by a Rushton impeller have been explored in detail by using image capturing and processing techniques. We found three kinds of typical particle suspension motions, namely, the lightest PMMA particle first moves upward from the bottom center of the tank to a certain height and then spirals up to the impeller, the heavier POM particle rises to a certain height vertically and then it spirals down to the tank bottom, the still heavier PTFE and glass particles jump at random when they are rolling irregularly on the tank bottom. The single-phase flow field of the stirred tank was measured by using 2D-PIV technique to address the mechanism of the particle lift-off. The random distribution of the regions with larger liquid velocity closely above the tank bottom might be the reason why the PTFE and glass particles were lifted off randomly. As for the PMMA and POM particles being lifted from the bottom center and then stagnating at a certain height, the bulk flow dominates the particle suspension.

KEYWORDS

PIV, solid–liquid suspension, stirred tank, transitional flow

1 | INTRODUCTION

Stirred tanks with solid–liquid mixtures are particularly common in chemical production and are also widely used in other industrial operations. Examples are the industrial crystallization process,[1] sludge treatment of wastewater,[2] solid–liquid mass transfer process in biological fermentation tank,[3] and heterogeneous catalysis.[4] The main purpose of solid–liquid suspension in stirred reactors is to make solid particles completely or uniformly dispersed in a liquid. This then increases the interphase contact area and enhances the solid–liquid mass transfer or catalytic process. Therefore, the research on solid–liquid suspension is of great significance.

Based on a large number of experiments, Zwietering[5] defined the impeller speed required for the solid particles to detach from the bottom of the stirred tank as the just-suspended speed (N_{js}) for the first time. The criterion for suspension of particles is that the static time of solid particles at the bottom of the tank shall not exceed 1–2 s. The criterion is still used to judge whether solid particles are in a suspended state. Zwietering analyzed the relationship of impeller type, impeller size and installation position, reactor size, particle size and concentration of solid particles, density and viscosity of the liquid on the just-suspended speed through experiments. The correlation proposed by Zwietering has some shortcomings. For example, the factors such as the off-bottom clearance of the turbine were not well considered, so many

subsequent researchers[6] proposed extensions. Armenante et al[7] determined the influence of impeller clearance, impeller diameter, and other operating variables on the just-suspended speed required for solids suspension.

Brucato et al[8] conducted solid–liquid suspension experiments in unbaffled stirred tanks. The steady-state cone radius method is used to determine the minimum impeller speed for which the solids are completely lifted off. The experimental results show that the influence of impeller speed on power (number) increases with the increase of solids loading and particle size, and the power consumption of the unbaffled stirred tanks is smaller than that of a baffled stirred tank. These researches pay more attention to the study of macroscopic characteristics in stirring tanks.

At present, the mechanism of solid particle suspension from the bottom is controversial. There are three dominant views: The first is the view from turbulence theory[9]; that is, the turbulent vortices play a major role in particle suspension. The second is the bulk flow theory[10]; that is, the bulk flow at the bottom of the stirred tank plays a major role in particle suspension. The third is the comprehensive action theory; that is, turbulent vortex and bulk flow affect particle suspension at the same time and to a similar extent.[11]

With the development of flow field visualization technology, people can more clearly understand the flow field structure in the stirred tanks. Li et al[12] used two-dimensional particle image velocimetry (2D-PIV) and refractive index matching to study the characteristics of a solid–liquid turbulent flow field in a stirred tank with a pitched-blade turbine. The results show that the presence of particles reduces the average flow velocity and turbulent kinetic energy, and this phenomenon is more obvious with the increase of solid holdup. Unadkat et al[13] used fluorescent PIV to photograph the solid–liquid suspension system through filters of different colors and obtained information on solid–liquid two-phase velocity, turbulent kinetic energy, and particle concentration distribution in the stirred tanks.

There have been a few comprehensive studies on the suspension movement of a small number of particles under laminar flow conditions. Wang et al[14] explored the suspension characteristics of eight particles in the stirred tanks driven by a Rushton turbine under laminar flow conditions. It is found that the particles form a stable structure near the center of the tank bottom, which hinders the movement of particles so that the just-suspended speed increases. In order to address the particle entrainment mechanisms, Mo et al[15] investigated the suspension characteristics of a single sphere in stirred tank with laminar flow. A similar approach is taken in this study where we follow the scenario for entrainment of a single sphere but now in transitional flow. Different from Mo's works, our experiments were carried out under a more complex condition with a standard Rushton turbine instead of a rotating disk and with higher Reynolds numbers.

Therefore, the aims of this paper are in the first place to explore the lift-off motion characteristics of a single spherical particle in a stirred tank with transitional flow. The typical motions are reported. In the second place, we use 2D-PIV to analyze the single-phase velocity fields in the tank and explain the particle suspension mechanism from the perspective of velocity fields.

2 | MATERIAL AND METHODS

2.1 | Experimental setup

The experiments were performed in a transparent rectangular stirred tank, as shown in Figure 1. The side length of the tank is $T = 0.22$ m. The stirred tank was filled with a silicone oil with density $\rho = 965\ \mathrm{kg/m^3}$ and liquid height $H = T$. The standard Rushton turbine with diameter $D = 0.5T$ was selected for the experiments. Two off-bottom clearances, $C = 1/3T$, and $C = 1/4T$ were selected for the Rushton turbine.

Four spherical particles all having diameter $d_p = 0.01$ m were considered in the experiments, namely, polymethyl methacrylate (PMMA) particle, polyoxymethylene (POM) particle, polytetrafluoroethylene (PTFE) particle, and glass particle. Their densities are 1208, 1351, 2200, and 2482 $\mathrm{kg/m^3}$, respectively. Given these densities, the net gravity force on the particles covers a significant range. The particles are also sufficiently robust to withstand collisions with impeller and

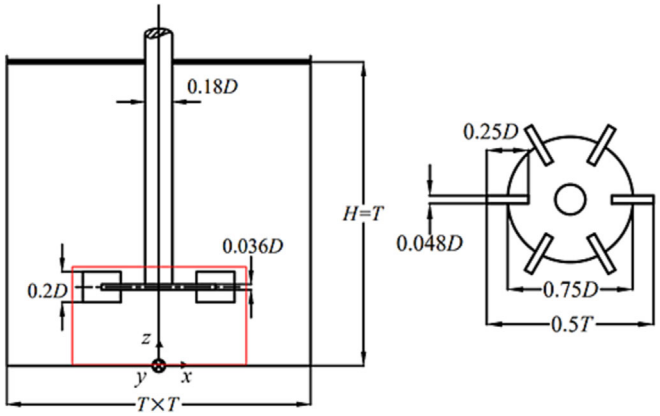

FIGURE 1 Geometry of stirred tank and impeller. A glass plate was used on the liquid surface to prevent air entrainment. The red rectangle represents the measurement plane of the 2D-PIV experiments. The origin of the Cartesian coordinate system is located at the center of the tank bottom.

tank walls. The particle surface was sprayed with a layer of white paint for clear identification. In each experiment, only one of the four particles was used and placed at the initial position (0.0, $-0.5D$, $0.5d_p$).

Silicone oil is Newtonian fluid, and it has good stability and transparency, which meets the requirements of the visualization experiment. The viscosity of the silicone oil was measured by a MARS40 rheometer (Haake, Germany). The average temperature was controlled at 25.7 ± 0.1°C, and the viscosity of the silicone oil at this temperature is 88.9 ± 0.2 mPa·s.

The impeller is driven by an electric motor (ABB, Switzerland), and its speedwas controlled by a 6SL3210 frequency converter (Siemens, Germany). An overview of the in total 23 experimental cases considered in this article is given in Table 1. When the particle is lifted off only once within 60 s and cannot be lifted off anymore (within 60 s and within any time larger than 60 s), the corresponding impeller speed is defined as $N_{LO,1}$. When the particle is lifted off at least one time within 60 s and can be lifted off repeatedly after its first lift-off, the corresponding impeller speed is defined as $N_{LO,m}$. When the particle randomly jumps up from the bottom and quickly comes back to the bottom within 60 s, the corresponding impeller speed is defined as $N_{LO,R}$. The Reynolds number is defined as $\mathrm{Re} = \rho N D^2/\mu$ with N the rotational speed of the impeller. For the sake of conciseness, we do not label the Reynolds numbers in different suspension processes as different symbols.

TABLE 1 Experimental parameters and results for the lift off impeller speed $N_{LO,1}$, $N_{LO,m}$, and $N_{LO,R}$.

Case	Particle	ρ_p/ρ	C/T	N (rpm)	Re
E1	PMMA	1.25	1/3	152 ($N_{LO,1}$)	337
E2				164 ($N_{LO,m}$)	359
E3				175	383
E4			1/4	142 ($N_{LO,1}$)	311
E5				144 ($N_{LO,m}$)	316
E6				163	356
E7				185	405
E8				213	467
E9	POM	1.40	1/3	172 ($N_{LO,1}$)	376
E10				180 ($N_{LO,m}$)	394
E11				198	433
E12			1/4	164 ($N_{LO,m}$)	360
E13				189	414
E14				213	466
E15	PTFE	2.28	1/3	218 ($N_{LO,R}$)	478
E16				283	619
E17				327	716
E18			1/4	226 ($N_{LO,R}$)	495
E19				294	644
E20	glass	2.57	1/3	230 ($N_{LO,R}$)	503
E21				299	654
E22			1/4	238 ($N_{LO,R}$)	521
E23				309	678

2.2 | High-speed imaging system

The motions of particles were captured by using two high-speed cameras (JAI GO-USB-5000M, Japan), as shown in Figure 2. In the experiment, the two cameras were located at the side and underneath the stirred tank, respectively, and filmed synchronously. The bottom camera was used to record the bottom paths of the particles, and the side camera was used to record the rising paths of the particles. Then, the 3D trajectory of the particle could be reconstructed; see Appendix S1. A 500-W square LED lamp was adopted as the light source. Considering data processing requirements, we used a resolution of 1280×1024 pixel^2 and a frame rate of 100 frames per second (fps) to capture the particle paths.

In this study, the images were processed in the MATLAB environment (version R2017a, Mathworks). First, the Canny edge detector[16] is used to find the region with the strongest change in image intensity to obtain the edge lines of the particle. Then, the edge lines are connected by using Circular Hough Transform (CHT),[17,18] and coordinates of the particle center can be obtained. After that, all data were processed and the particle velocity was calculated from particle location data by using Central Differences.[19]

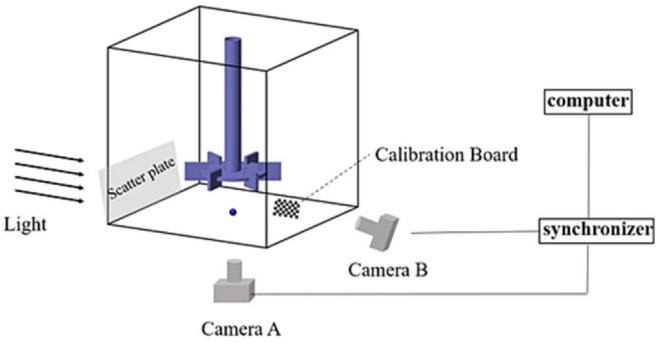

FIGURE 2 Optical layout. The spatial positions of the camera, light source, and calibration board are shown schematically. Two cameras film the calibration board or particle movement at the same time.

2.3 | Single-phase 2D PIV

A 2D PIV system (TSI, USA) was used to measure the velocity of the single-phase flow field in the tank. The system consists of an Nd:YAG dual-pulse laser (532 nm, 200 mJ, Vlite-200, Beamtech, China), a CCD camera (PowerView Plus 11 M, TSI), a synchronizer (Laser Pulse 610035, TSI), a shaft encoder (A02H, Kubler, Germany), and a computer with TSI INSIGHT 4G processing software. The tracer particles used in the experiment are hollow glass beads 8–12 μm in diameter. In the experiment, the lens of the CCD camera is 180 mm and the resolution is 4008 × 2672 pixel^2, and the minimum shooting distance is 47 mm. Impeller angle resolved experiments were performed by using the encoder, and then angle resolved as well as angle-averaged flow fields were obtained.

In the experiments, the cross-correlation algorithm based on the Fast Fourier Transform was used to process the instantaneous images of tracer particles in two frames, and the instantaneous velocity distribution of the fluid is obtained. The method has the advantages of background noise reduction, high signal-to-noise ratio, and high effective particle number.[20] The resolution of any two successive vectors in our experimental data is 0.61 mm.

3 | RESULTS AND DISCUSSION

3.1 | Critical lift-off speeds of particles

Table 2 shows the critical impeller speeds to lift off particles as a function of the dimensionless off-bottom clearance of the impeller. In our experiments, the lift-off speed of each particle was roughly determined by using the bisection method first, and then the speed was increased or decreased by 2% to check the lift-off condition of the particle until the critical lift-off speed, such as $N_{LO,1}$, $N_{LO,m}$, or $N_{LO,R}$, was determined. Each experiment has been repeated at least two times to confirm the reproducibility.

TABLE 2 Critical lift-off speed of four particles at different off-bottom clearance of impeller.

Particle	ρ_p/ρ	C/T	$N_{LO,1}$	$N_{LO,m}$	$N_{LO,R}$
PMMA	1.25	1/3	152	164	
		1/4	142	144	
POM	1.40	1/3	172	180	
		1/4		164	
PTFE	2.28	1/3			218
		1/4			226
glass	2.57	1/3			230
		1/4			238

For the PMMA particle, $N_{LO,1}$ and $N_{LO,m}$ increase with increasing C/T. Similar result could be found for the $N_{LO,m}$ of the POM particle. We did not observe the phenomena that the POM particle could be lifted off only once at $C = 1/4T$. As for the PTFE and glass particles, $N_{LO,R}$ decreases with increasing C/T.

3.2 | Bottom motion of particles

Figure 3 shows the trajectories of the particles rolling on the tank bottom. In the visualization experiments, we used the same acceleration of 100 rpm/s as that in Mo's work.[15] For example, in case E20 with glass particle and critical impeller speed of 230 rpm, we started the stationary impeller at $t = 0$ with the acceleration of 100 rpm/s, and it took the impeller 2.3 s to reach the target speed of 230 rpm. During the process, the number of impeller revolutions was 2.3 * 230/60/2 = 4.41.

For the PMMA particle, the Reynolds number has negligible effect on its trajectory, as shown in Figure 3a. When Re ranges from 316 to 356, 405, and 467, the dimensionless time tN it takes for the particle to move from the initial position to a location within a distance of d_p from the bottom center decreases from 12.0 to 11.2, 10.1, and 9.8, respectively. That is, for the PMMA particle, to travel the same distance on the tank bottom, the higher the Re, the lower the total impeller revolutions required. Similar phenomena could be observed for the POM particle when Re ranges from 360 to 466; see Figure 3b and Table 1. Figure 3b also shows that the heaviest glass particle with $\rho_p/\rho = 2.57$ and Re = 521 follows a longer and more curved path than other particles, which is different from previous research where the lighter the particle, the longer and more curved the trajectory.[15] As for the effect of impeller off-bottom clearance, Figure 3c,d shows that a more curved trajectory is followed at higher clearance, which is in contradiction with previous laminar flow as well.[15] It is also interesting that the higher the clearance the lower the Re for the lift-off of the PTFE and glass particles. The reasons might be the transformation from the laminar flow into the transitional flow with increasing Reynolds number, as well as the use of the Rushton turbine instead of the rotating disk in Mo et al.[15]

3.3 | Lift-off motion of particles in stirred tank

3.3.1 | Lift-off trajectories of glass and PTFE particles

In laminar flow, if a spherical particle rolls to the center of tank bottom, it then gets lifted off right there, hits the

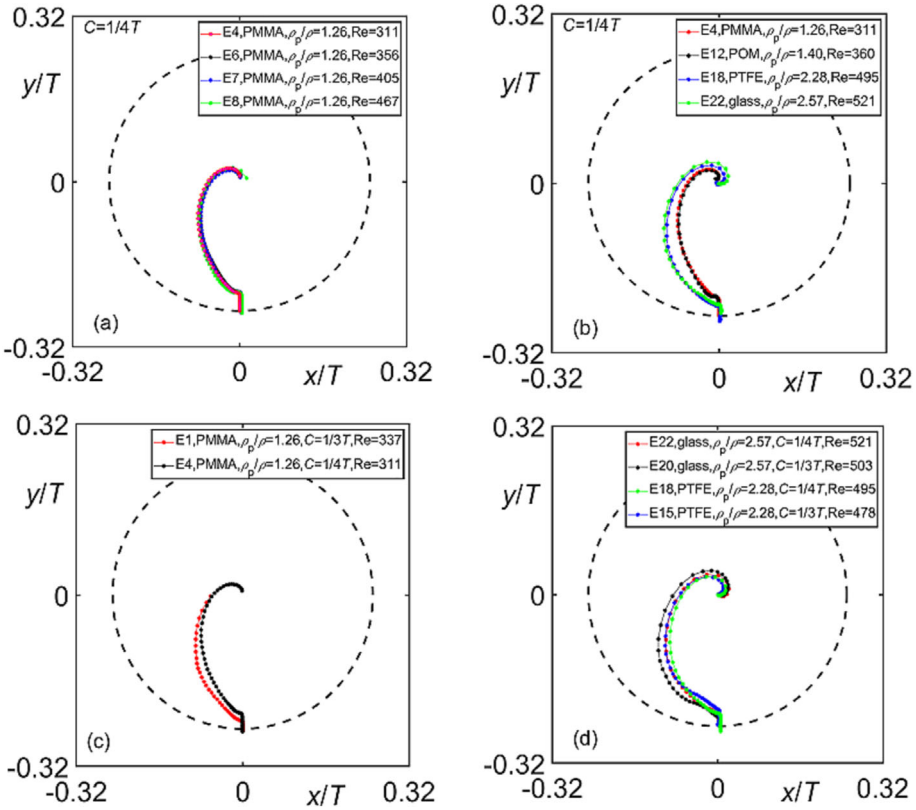

FIGURE 3 Trajectories of particles rolling on the tank bottom. (a) Effect of Re at $C = 1/4T$; (b) effect of particle density at $C = 1/4T$; (c,d) effect of impeller off-bottom clearance.

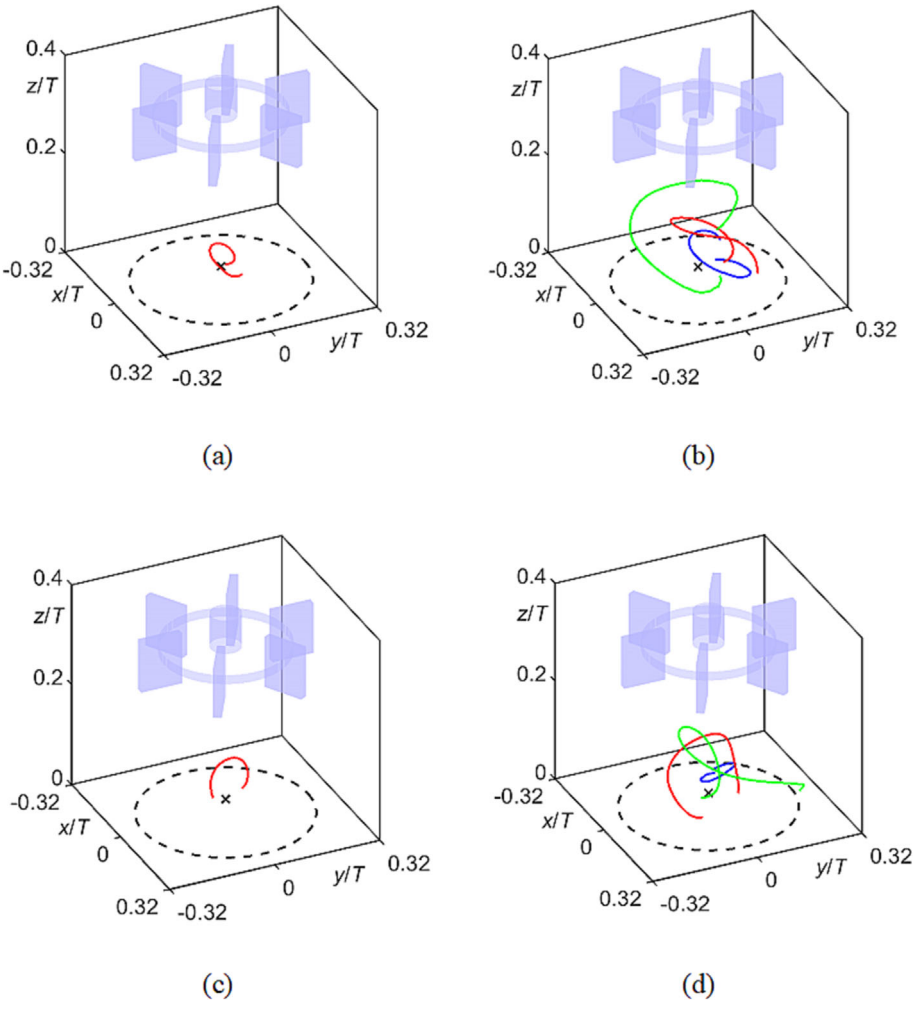

FIGURE 4 Lift-off trajectories of glass and PTFE particles at $C = 1/3T$. (a) Case E15, PTFE, Re = 478; (b) case E16, PTFE, Re = 619; (c) case E20, glass, Re = 503; (d) case E21, glass, Re = 654. The PTFE and glass particles could be lifted off only once within 60 s at Re = 478 and Re = 503, as shown in panels (a) and (c). As Reynolds number increases to 619 and 654, the PTFE and glass particles could be lifted off several times within 60 s. Only three lift-off trajectories in different colors are illustrated in panels (b) and (d). The dashed circle on the bottom wall in each panel, with diameter of D, is used for reference. A marker with coordinate $(0, 0, 0.5d_p)$ is shown in each panel.

lower surface of the impeller, spirals around and is eventually swirled out.[15] In transitional flow, however, we observed different phenomena, as shown in Figures 4 and 5. For example, at critical impeller speed $N_{LO,R}$, the glass particle rolls to the near center of tank bottom first (see Figure 3), but then it moves spirally around the center, as illustrated in Figure 5a,b. During the latter process, the glass particle jumps randomly from the tank bottom, travels along irregular trajectory, and then comes back to the bottom wall again, as shown in Figure 4c. The PTFE particle behaves in similar way. With increasing Re, the jump height, jump frequency, and trajectory length increase simultaneously; see Figure 4b,d.

As shown in Figure 5a,b, the trajectories of the glass particle on the bottom wall, including projected trajectories when the particle jumps, are random. With the increase of Re, the particle spirals further away from the bottom center. To quantitatively describe the bottom motion, time series of the dimensionless distance s_i/D between particle center and the center of tank bottom are shown in Figure 5c,d. The average distances $\bar{s}/D$ for the two experiments E22 and E23 are 0.0984 and 0.1941, respectively. Standard deviations σ of the distances s_i/D (see Equation 1) in E22 and E23 are 0.0449 and 0.1258, respectively.

$$\sigma(s_i/D) = \sqrt{\frac{\sum_{i=1}^{n}((s_i - \bar{s})/D)^2}{n-1}} \quad (1)$$

where n is the number of samples, that is, the number of frames the trajectory is determined from. With increasing Re from 521 of E22 to 678 of E23, the average distance almost doubles (from 0.0984 to 0.1941), and the standard deviation of the distance increases by 2.8 times (from 0.0449 to 0.1258). We then speculate that fluctuating fluid velocity plays an importance role in lifting off the glass particle. As for the PTFE particle, we observe similar results in the experiments.

3.3.2 | Lift-off trajectories of PMMA and POM particles

Figure 6a,b show the lift-off trajectories of the PMMA particle at two Reynolds numbers. At critical lift-off speed $N_{LO,1}$ of 152 rpm with Re = 337, the PMMA particle is suspended first from the center of the tank bottom, and then it moves along a perfectly vertical line to a height of $z/T = 0.17$. After that, the particle will stay right there for about 5 impeller revolutions. Then, the particle spirals

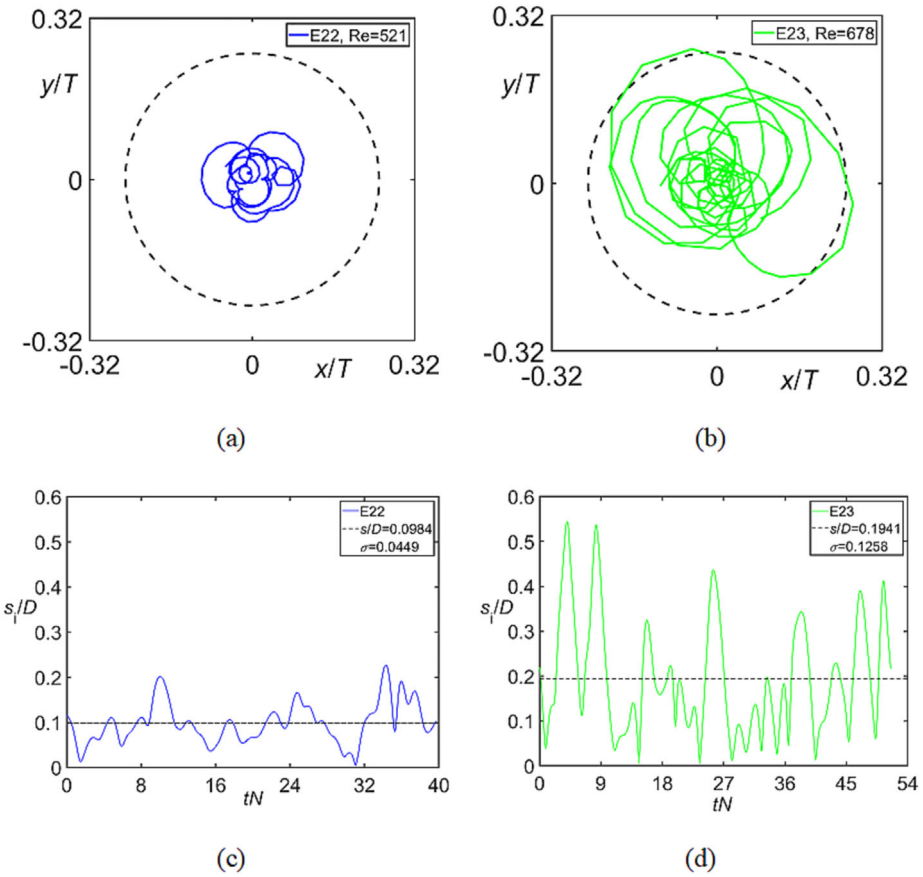

FIGURE 5 (a,b) Projected trajectories followed by the glass particle ($\rho_p/\rho = 2.57$) during a time period of 10 s on a plane $z = 0.5\ d_p$ in two experiments E22 and E23. (c,d) Dimensionless distance between particle center and the center of tank bottom as a function of dimensionless time tN.

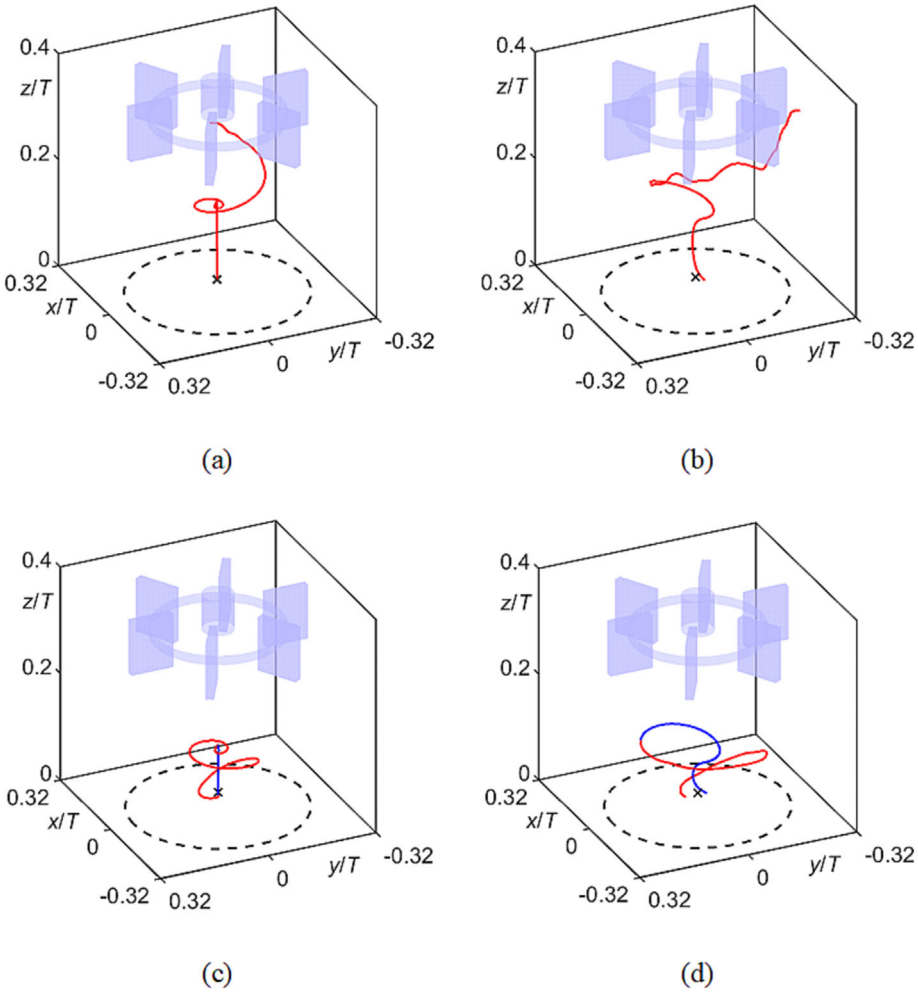

FIGURE 6 Lift-off trajectories of the PMMA and POM particles at $C = 1/3T$. (a) Case E1, PMMA, Re = 337; (b) case E3, PMMA, Re = 383; (c) case E9, POM, Re = 376; (d) case E11, POM, Re = 433. The up and down motions of the POM particle in panels (c) and (d) are illustrated by using blue and red lines, respectively. The dashed circle on the bottom wall in each panel, with diameter of D, is used for reference. A marker with coordinate $(0, 0, 0.5d_p)$ is shown in each panel.

upwardly and outwardly. We stopped displaying the trajectory if the particle collided with the impeller, as shown in Figure 6a. When impeller speed was increased to 175 rpm with Re = 383, the location where the particle was lifted off is about 3 mm away from the bottom center. Moreover, the lift-off trajectory becomes more curved and fluctuating with increasing Re; see Figure 6b.

For the POM particle, similar phenomena could be observed except that the POM particle moves downward to the tank bottom instead of upward to the impeller after it is lifted to a certain height, as illustrated in Figure 6c,d. Overall, the lift-off patterns and trajectories of the PMMA and POM particles are different from those of the glass and PTFE particles, compare Figures 4 and 6. They are different from the results in laminar flow as well.[15] Various particle trajectories presented in this study could provide experimental data for future numerical verifications. Particle motion is eventually related to the flow field, and we will investigate the relation between flow and particle motion in the next section.

Figure 7 shows the time series of particle trajectory and particle vertical velocity. At Re = 337, the PMMA particle was lifted off to a height around $z/C = 0.5$ first, and then it slightly went down and almost stayed there for several impeller revolutions until it spiraled toward the impeller. As it is difficult to identify the particle when it moved behind the impeller blade or collided with the blade, the trajectory is not displayed after the particle approaches the lower edge of the blade, which is illustrated as the dashed line in Figure 7a. With increasing Re, the stagnation height of the PMMA particle decreases, and the particle spends much less time at the stagnation position.

Before the stagnation position, a very clear velocity peak could be observed for the two experiments E1 and E2, as shown in Figure 7c. The velocity fluctuation near the end of the profile is caused by the interaction between the particle and the impeller blade.

In terms of stagnation height at about constant Re, such as 383 and 376, we can find that the stagnation height of the POM particle is smaller than that of the PMMA particle; see Figure 7a,b. Further increasing Re to 433, the stagnation phenomenon of the POM particle disappears, which might be caused by the instability of the

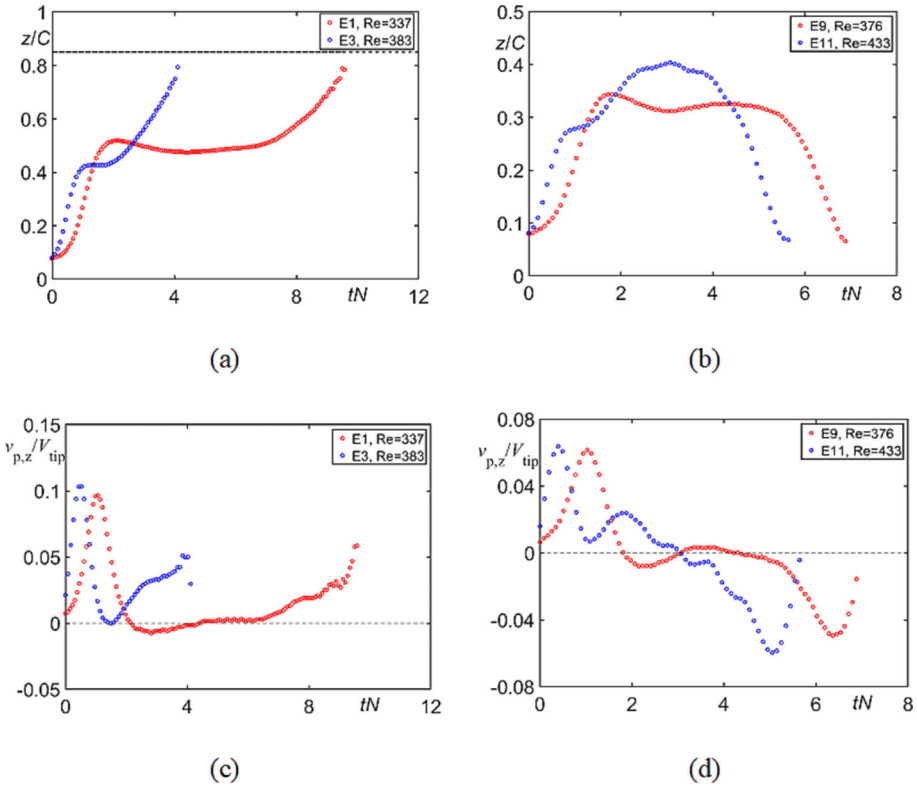

FIGURE 7 Time series of particle trajectory (top row) and vertical velocity (bottom row) at $C = 1/3T$ for the PMMA particle (left column) and for the POM particle (right column). The dashed line in panel (a) shows the lowest edge of the impeller, where collisions between particles and the blade might happen. The moment with the gap between tank bottom wall and particle of 0.1 d_p is defined as $t = 0$.

flow field at Re = 433. At the two Reynolds number of 376 and 433, the POM particle eventually comes back to the tank bottom instead of moving upwardly to the impeller. Thus, besides the initial velocity peak, we can also observe a second velocity valley near the end of the time series.

3.4 | Analysis of flow field in stirred tank

Single-phase flow field in the stirred tank was measured and analyzed to address the mechanism of particle suspension. We selected one operating condition with Re = 716 and $C = 1/3T$ for showing the variation of instantaneous flow fields; see Figure 8. Both the velocity vectors and the velocity magnitude contours illustrate that the instantaneous velocity field changes constantly and quickly even at the same impeller angle, as shown in Figure 8a,b, even more so with different impeller angles. However, the angle-resolved average flow field and the angle-averaged flow field (see Figure 8c–f) are almost symmetrical. If we only would look at the experimental angle-resolved or angle-averaged data, which could also be obtained in numerical simulations based on Reynolds-averaged Navier–Stokes models, it would be hard to imagine the particle movement described in Section 3.3. Thus, the instantaneous velocity field could present more useful insight into understanding the lift-off motion in Section 3.3.1 for the heavier PTFE and glass particles. That is, the irregular and random instantaneous flow fields, instead of angle-resolved or angle-averaged flow fields, trigger the intermittent lift-off of the PTFE and glass particles. Figure 8c–f also shows that angle-resolved and angle-averaged results only differ significantly near the impeller blades.

Figure 9 shows four instantaneous velocity fields in stirred tank at Re = 383 and $C = 1/3T$. The streams moving inward along the tank bottom induce a strong upward flow in the center of the tank toward the impeller. The upward stream diverges at a certain height. We observe a region with weak flow between the disk of the impeller and the height of divergence. Although the streams and their merging and diverging are slightly different as a function of time, the region with weak flow always exist, and the stagnation points of the PMMA and POM particles are at the bottom of the region, as indicated in Figure 9.

The drag force—which in this situation is by far the strongest hydrodynamic force on the particle—in z direction is expressed as

$$F_{d,z} = \frac{\pi}{8} C_D \rho d^2{}_p \left(v_{p,z} - v_z\right)^2 \quad (2)$$

C_D is calculated by the following equation[21]:

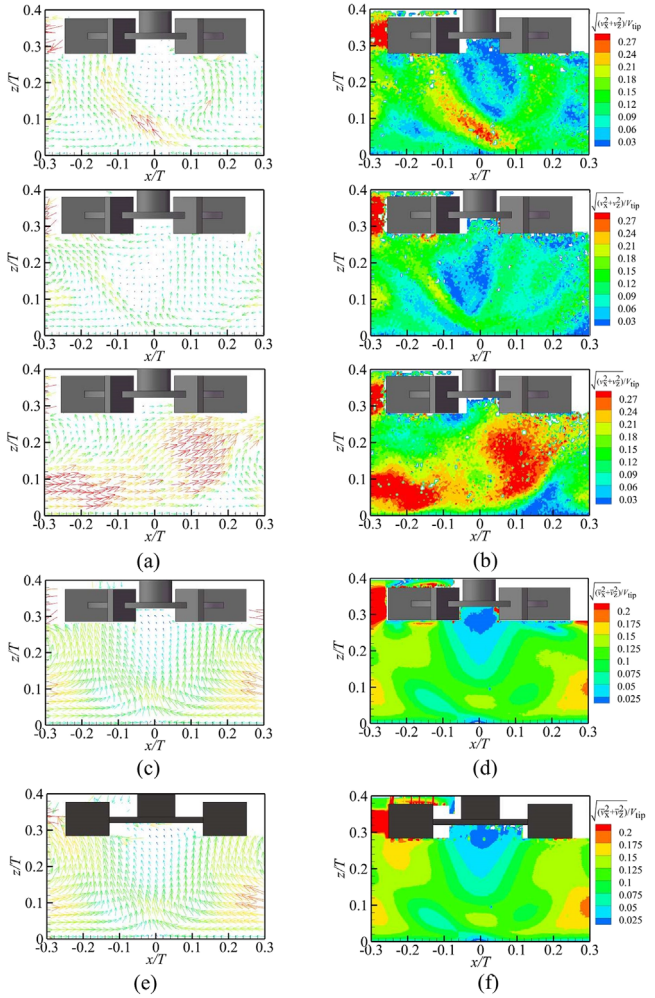

FIGURE 8 Three instantaneous velocity vector fields (a) and contour fields (b) at impeller angle of 0° as indicated by the impeller model in each panel. Angle-resolved average velocity vector field (c) and contour field (d) at impeller angle of 0° based on 500 instantaneous flow fields. Angle-averaged velocity vector field (e) and contour field (f) based on 1500 instantaneous flow fields at three impeller angles of 0°, 20°, and 40°. Re = 716 and $C = 1/3T$.

$$C_D = \frac{24}{\mathrm{Re}_p}\left[1 + 0.1315\,\mathrm{Re}_p^{(0.82-0.05\log_{10}\mathrm{Re}_p)}\right] (0.01 < \mathrm{Re}_p < 20) \quad (3)$$

$$\mathrm{Re}_p = \frac{d_p|v_{p,z} - v_z|\rho}{\mu} \quad (4)$$

The threshold for lifting off a particle is as follows:

$$F_d - G_{net} = \frac{\pi}{8} C_D \rho d_p^2 \left(v_{p,z} - v_z\right)^2 - \frac{\pi}{6} d_p^3 \left(\rho_p - \rho\right) g > 0 \quad (5)$$

The particle velocity at its stagnation point is considered as zero. Then solid–liquid slip velocity in z direction is the local liquid velocity in z direction. From Figures 9 and 10, we obtain the latter, and they are about

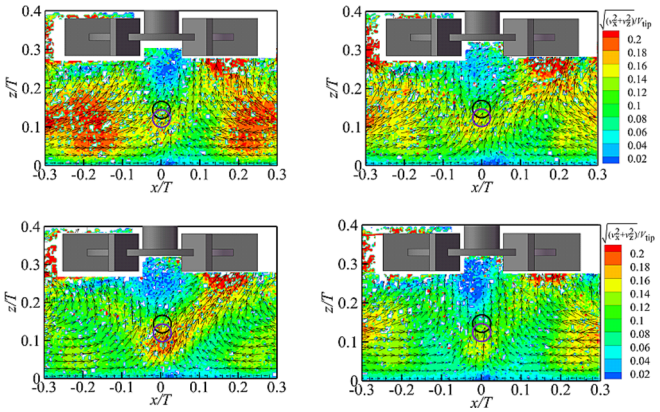

FIGURE 9 Four instantaneous velocity fields in stirred tank at $C = 1/3T$ and Re = 383. Black circle in each panel represents the stagnation position of the PMMA particle, and purple circle that of the POM particle.

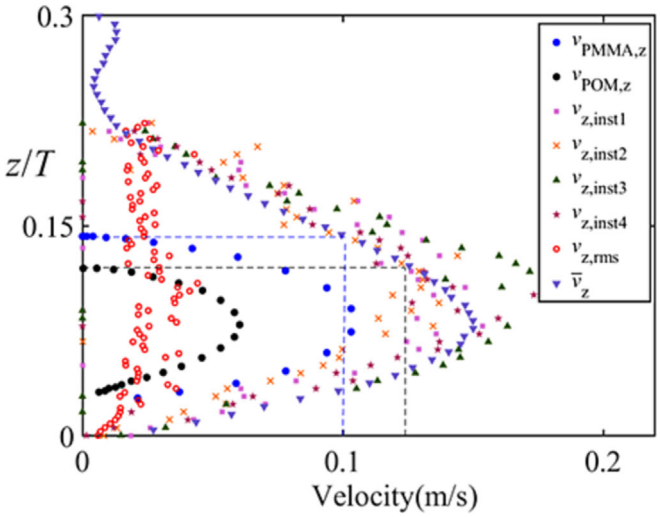

FIGURE 10 Profiles of velocity component in z direction, including PMMA particle velocity component at Re = 383, POM particle velocity component at Re = 375, four instantaneous liquid velocity component at Re = 383, rms of liquid velocity fluctuation component at Re = 383, and phase-averaged liquid velocity component at Re = 383. The dashed lines show that at the stagnation points of the PMMA and POM particles, the average liquid velocity component in z direction are about 0.10 and 0.12 m/s, respectively. $C = 1/3T$, $x/T = 0$.

0.10 and 0.12 m/s for the PMMA particle and POM particle, respectively. Based on Equations (2)–(4), the drag coefficients C_D for the two particles are $C_{D,PMMA} = 4.03$ and $C_{D,POM} = 3.56$, and the drag forces for the two particles at their stagnation points have been calculated as $F_{d,PMM\ A} = 1.53 \times 10^{-3}$ N and $F_{d,POM} = 1.94 \times 10^{-3}$ N. The net gravity of the two particles are $G_{net,PMMA} = 1.25 \times 10^{-3}$ N and $G_{net,POM} = 1.98 \times 10^{-3}$ N. The estimation of drag force

and comparison between drag force and net gravity could explain why particle stagnates at a certain height. It should be mentioned that the estimation based on one-dimensional flow and particle motion (both in z direction) is a fair approximation given the mostly vertical flow at the location of interest and the mostly vertical particle motion.

In a similar way, we approximately infer that drag force in z direction overcomes the net gravity of the PMMA particle after its stagnation as it continues moving upwardly, while the net gravity of the POM particle dominates in z direction after the stagnation because it comes back to the tank bottom. Actually, the forces acting on the particles are complicated and three dimensional, inducing the 3D particle trajectories in Figure 6.

Ayranci et al[11] reported that at a high Reynolds number, the bulk flow and turbulent vortices act simultaneously on the particle suspension process. Figure 10 shows profiles of velocity components in z direction of two particles and the liquid along the center line of the tank. At each z/T, the instantaneous velocities fluctuate around the average velocity, with low level of root mean square (rms) velocity, which means the flow field at $x/T = 0$ is dominated by the bulk flow at Re = 383. After the particle is lifted off from the tank bottom, it follows the liquid flow, moving toward the impeller. The heavier the particle, the larger the slip velocity between the particle and the liquid. At about the same axial position $z/T = 0.08$, the velocity components of the liquid, the PMMA particle, and the POM particle reach their corresponding maxima. Then, the liquid velocity component decreases with increasing axial position z/T, and the particle velocity component decreases as well. When the liquid field cannot generate sufficient force to lift the particle, the particle stagnates at certain axial position, as shown in Figure 6. Therefore, it is inferred that the particle suspension in this study is mainly related to the bulk flow.

4 | CONCLUSIONS

In this work, the suspension characteristics of a single spherical particle in a mixing tank equipped with a Rushton turbine under transitional flow conditions were investigated. The 2D-PIV technique was used to measure the velocity of the single-phase flow field of the tank. The reasons for different particle suspension movements are explained from the perspective of the flow field.

For the lighter PMMA and POM particles with density ratios of 1.25 and 1.4, respectively, the variety of Re hardly affects the particles motion. The dimensionless time tN required for particles to roll to the center of tank bottom decreases with increasing Re. The heaviest glass particle with density ratios of 2.57 followed a much longer and more curved path than the other particles. A more curved path is also followed at higher impeller clearance.

The paths of particles suspension motion are divided into three categories: (1) The lightest PMMA particle first moves upward from the bottom center of the tank to a certain height, and then spirals up to the bottom of the impeller; (2) the heavier POM particle rises to a certain height vertically, and then it spirals down to the bottom of the tank; (3) the still heavier PTFE and glass particles jump at random when they are rolling irregularly on the bottom wall of the tank.

The single-phase flow in the stirred tank was analyzed to explain the reasons for the particle suspension characteristics. The random nature of high-velocity regions as observed in subsequent PIV images might be the reason why the PTFE and glass particles were lifted off randomly. There is a region with on average weak flow between the disk of the impeller and the diverging stream, where the PMMA and POM particles being lifted from the tank bottom stop rising. Quantitative force balance analysis regarding the PMMA and POM particles shows that instantaneous liquid velocity and the corresponding drag force distribution determine the lift-off trajectories of the particles. Comparisons of different velocity profiles further confirm the effect of the bulk flow on the particle suspension.

Various particle suspension patterns are reported in the current study, which could be utilized for future numerical simulations and validations. Further increasing the Reynolds number of the flow field or using different particle shape or various impellers would be another research direction for future work.

NOMENCLATURE

C	off-bottom clearance of the Rushton turbine [m]
C_D	drag coefficient [−]
D	impeller diameter [m]
d_p	particle diameter [m]
$F_{d,z}$	drag force in z direction [N]
g	gravitational acceleration [m/s^2]
G_{net}	net gravity [N]
H	liquid height inside the tank [m]
N	impeller speed [revolution/s]
N_{LO}	lift-off impeller speed [revolution/s]
Re	Reynolds number based on impeller speed, $\mathrm{Re} = \rho N D^2/\mu$ [−]
Re_p	particle Reynolds number [−]
s_i	instantaneous distance between particle center and tank bottom center [m]
$\bar{s}$	average distance between particle center and tank bottom center [m]
t	time [s]

T	side length of the tank [m]
$v_{p,z}$	particle velocity component in z direction [m/s]
v_x	instantaneous liquid velocity component in x direction [m/s]
v_z	instantaneous liquid velocity component in z direction [m/s]
$\overline{v}_x$	averaged liquid velocity component in x direction [m/s]
$\overline{v}_z$	averaged liquid velocity component in z direction [m/s]
$v_{z,rms}$	root mean square (rms) of liquid velocity fluctuation in z direction v_z-$\overline{v}_z$ [m/s]
V_{tip}	impeller tip velocity [m/s]
x, y, z	Cartesian coordinates [m]

GREEK LETTERS

ρ	density of the silicone oil [kg/m^3]
ρ_p	density of particle [kg/m^3]
σ	standard deviation [−]
μ	viscosity of the silicone oil [Pa·s]

ACKNOWLEDGEMENTS

The authors gratefully acknowledge the financial support from Scientific Research and Technology Development Projects of China National Petroleum Corporation (No. 2020B-2512).

ORCID

Jianghao Wang https://orcid.org/0009-0007-0833-5402
Zhipeng Li https://orcid.org/0000-0003-1450-8836

REFERENCES

1. Akrap M, Kuzmanic N, Kardum JP. Impeller geometry effect on crystallization kinetics of borax decahydrate in a batch cooling crystallizer. *Chem Eng Res Des*. 2012;90(6):793-802. doi:10.1016/j.cherd.2011.09.015
2. Bai LL, Wang CH, Pei YS, Zhao JB. Reuse of drinking water treatment residuals in a continuous stirred tank reactor for phosphate removal from urban wastewater. *Environ Technol*. 2014;35(21):2752-2759. doi:10.1080/09593330.2014.920050
3. Kasat GR, Pandit AB. Review on mixing characteristics in solid-liquid and solid-liquid-gas reactor vessels. *Can J Chem Eng*. 2015;83:618-643.
4. Muñoz JA, Dreisinger DB, Cooper WC, Young SK. Silver-catalyzed bioleaching of low-grade copper ores. Part II: stirred tank tests. *Hydrometallurgy*. 2017;88:19-34.
5. Zwietering TN. Suspending of solid particles in liquid by agitators. *Chem Eng Sci*. 1958;8(3-4):244-253. doi:10.1016/0009-2509(58)85031-9
6. Ayranci I, Kresta SM. Critical analysis of Zwietering correlation for solids suspension in stirred tanks. *Chem Eng Res Des*. 2014;92(3):413-422. doi:10.1016/j.cherd.2013.09.005
7. Armenante PM, Nagamine EU, Susanto J. Determination of correlations to predict the minimum agitation speed for complete solid suspension in agitated vessels. *Can J Chem Eng*. 1998;76(3):413-419. doi:10.1002/cjce.5450760310
8. Brucato A, Cipollina A, Micale G, Scargiali F, Tamburini A. Particle suspension in top-covered unbaffled tanks. *Chem Eng Sci*. 2010;65(10):3001-3008. doi:10.1016/j.ces.2010.01.026
9. Baldi G, Conti R, Alaria E. Complete suspension of particles in mechanically agitated vessels. *Chem Eng Sci*. 1978;33(1):21-25. doi:10.1016/0009-2509(78)85063-5
10. Einenkel WD. Influence of physical properties and equipment design on the homogeneity of suspensions in agitated vessels. *German J Chem Eng*. 1980;3:118-124.
11. Ayranci I, Machado MB, Madej AM, Derksen JJ, Nobes DS, Kresta SM. Effect of geometry on the mechanisms for off-bottom solids suspension in a stirred tank. *Chem Eng Sci*. 2012;79:163-176. doi:10.1016/j.ces.2012.05.028
12. Li G, Li Z, Gao Z, Wang J, Bao Y, Derksen JJ. Particle image velocimetry experiments and direct numerical simulations of solids suspension in transitional stirred tank flow. *Chem Eng Sci*. 2018;191:288-299. doi:10.1016/j.ces.2018.06.073
13. Unadkat H, Rielly CD, Hargrave GK, Nagy ZK. Application of fluorescent PIV and digital image analysis to measure turbulence properties of solid-liquid stirred suspensions. *Chem Eng Res Des*. 2009;87(4):573-586. doi:10.1016/j.cherd.2008.11.011
14. Wang C, Zhang L, Li Z, Gao Z, Derksen JJ. Multi-particle suspension in a laminar flow agitated by a Rushton turbine. *Chem Eng Res Des*. 2018;132:831-842. doi:10.1016/j.cherd.2018.02.035
15. Mo J, Gao Z, Bao Y, Li Z, Derksen JJ. Suspending a solid sphere in laminar inertial liquid flow—experiments and simulations. *AIChE J*. 2015;61(4):1455-1469. doi:10.1002/aic.14756
16. Canny J. A computational approach to edge detection. *IEEE T Pattern Anal*. 1986;8(6):679-698. doi:10.1109/TPAMI.1986.4767851
17. Hough PVC. Method and means for recognizing complex patterns. USA Patent, 3069654. 1962.
18. Ioannou D, Huda W, Laine AF. Circle recognition through a 2D Hough transform and radius histogramming. *Image Vis Comput*. 1999;17(1):15-26. doi:10.1016/S0262-8856(98)00090-0
19. Dilloo MJ, Tangman DY. A high-order finite difference method for option valuation. *Comput Math Appl*. 2017;74(4):652-670. doi:10.1016/j.camwa.2017.05.006
20. Sung J, Yoo JY. Three-dimensional phase averaging of time-resolved PIV measurement data. *Meas Sci Technol*. 2001;12(6):655-662. doi:10.1088/0957-0233/12/6/301
21. Clift R, Grace JR, Weber ME. *Bubbles, drops, and particles*. Academic Press; 1978.

SUPPORTING INFORMATION

Additional supporting information can be found online in the Supporting Information section at the end of this article.

How to cite this article: Wang J, Huang F, Zhang K, et al. Suspension of a single sphere in a stirred tank with transitional flow. *Asia-Pac J Chem Eng*. 2023;18(4):e2910. doi:10.1002/apj.2910